AGU PUBLICATIONS

JGR

Journal of Geophysical Research: Solid Earth

RESEARCH ARTICLE
10.1002/2017JB014242

Key Points:
- Interpret measured streaming potential via history matching method at continuum level
- Propose an empirical power law model for the relative streaming charge density in sandstone
- Complex coupling coefficient behavior can be predicted by fitting the Q_v model

Supporting Information:
- Supporting Information S1
- Data Set S1

Correspondence to:
J. Zhang,
jiazuo.zhang11@imperial.ac.uk

Citation:
Zhang, J., J. Vinogradov, E. Leinov, and M. D. Jackson (2017), Streaming potential during drainage and imbibition, *J. Geophys. Res. Solid Earth*, *122*, 4413–4435, doi:10.1002/2017JB014242.

Received 29 MAR 2017
Accepted 29 MAY 2017
Accepted article online 1 JUN 2017
Published online 28 JUN 2017

Streaming potential during drainage and imbibition

Jiazuo Zhang[1], Jan Vinogradov[1,2], Eli Leinov[1,3], and M. D. Jackson[1]

[1]Department of Earth Science and Engineering, Imperial College London, London, UK, [2]Now at the School of Engineering, University of Aberdeen, Aberdeen, UK, [3]Now at the Department of Mechanical Engineering, Imperial College London, London, UK

Abstract The rock pore space in many subsurface settings is saturated with water and one or more immiscible fluid phases. Examples include nonaqueous phase liquids (NAPLs) in contaminated aquifers, supercritical CO_2 during sequestration in deep saline aquifers, the vadose zone, and hydrocarbon reservoirs. Self-potential (SP) and seismoelectric (SE) methods have been proposed to monitor multiphase flow in such settings. However, to properly interpret and model these data requires an understanding of the saturation dependence of the streaming potential. This paper presents a methodology to determine the saturation dependence of the streaming potential coupling coefficient (C) and streaming current charge density (Q_s) in unsteady state drainage and imbibition experiments and applies the method to published experimental data. Unsteady state experiments do not yield representative values of C and Q_s (or other transport properties such as relative permeability and electrical conductivity) at partial saturation (S_w) because S_w within the sample is not uniform. An interpretation method is required to determine the saturation dependence of C and Q_s within a representative elementary volume with uniform saturation. The proposed method makes no assumptions about the pore space geometry. Application of the method to published experimental data from two natural sandstone samples shows that C exhibits hysteresis between drainage and imbibition, can exhibit significant nonmonotonic variations with saturation, is nonzero at the irreducible water saturation, and can exceed the value observed at $S_w = 1$. Moreover, Q_s increases with decreasing S_w but is not given by $1/S_w$ as is often assumed. The variation in Q_s with S_w is very similar for a given sample and a given drainage or imbibition process, and the difference between samples is less than the difference between drainage and imbibition. The results presented here can be used to help interpret SP and SE measurements obtained in partially saturated subsurface settings.

1. Introduction

The pore space in many subsurface settings is saturated with water and another immiscible fluid phase; examples include nonaqueous phase liquids (NAPLs) in contaminated aquifers, the vadose zone, saline aquifers during CO_2 sequestration, and hydrocarbon reservoirs. Use of the self-potential (SP) and seismoelectric (SE) method has been proposed to monitor flow in such settings [e.g., *Antraygues and Aubert*, 1993; *Doussan et al.*, 2002; *Darnet and Marquis*, 2004; *Moore et al.*, 2004; *Jackson et al.*, 2005; *Linde et al.*, 2007; *Kulessa et al.*, 2012; *Saunders et al.*, 2012; *Talebian et al.*, 2013; *Warden et al.*, 2013; *Revil et al.*, 2014; *Jougnot et al.*, 2015]. However, to properly interpret and model these data requires an understanding of the saturation dependence of the streaming potential generation during two-phase flow.

When fluid in a porous rock is subjected to a pressure gradient that causes it to flow relative to the mineral surfaces, an excess of electrical charge within the so-called diffuse layer adjacent to the mineral surfaces is transported with the flow, leading to the generation of a streaming current. At a steady state, the streaming current is balanced by a conduction current to maintain electrical neutrality, and the associated electrical potential is termed the streaming potential [e.g., *Corwin and Hoover*, 1979; *Revil*, 1999; *Darnet et al.*, 2004; *Jackson*, 2008]. There is no requirement for the streaming and conduction currents to follow the same path except in the simple one-dimensional (1-D) case. The streaming current may be induced by a pressure gradient driving flow, which yields the streaming potential contribution to the measured SP, or a transient pressure gradient caused by seismic waves passing through the medium, which yields the SE effect.

At the continuum level, for single-phase flow, the Darcy velocity $\boldsymbol{q}$ (m s^{-1}) and the total current density $\boldsymbol{j}$ (A m^{-2}) are related to the gradients in fluid potential P (Pa) and electrical potential U (V) by [*Ishido and Mizutani*, 1981; *Jouniaux and Pozzi*, 1995]

$$\boldsymbol{j} = -\sigma\nabla U + L\nabla P \tag{1}$$

$$\boldsymbol{q} = -\frac{k}{\eta}\nabla P + L\nabla U \tag{2}$$

where σ (S m^{-1}) is the electrical conductivity of the porous medium, k (m^2) is the permeability, η (Pa s) is the viscosity of the fluid, and L (V S Pa^{-1} m^{-1}) is the electrokinetic cross-coupling term. At equilibrium the streaming and conduction currents balance in 1-D and the ratio of the pressure and voltage difference defines the streaming potential coupling coefficient [*Sill*, 1983]

$$C = \left.\frac{\Delta U}{\Delta P}\right|_{j=0} = -\left.\frac{L}{\sigma}\right|_{j=0} \tag{3}$$

where ΔU (V) and ΔP (Pa) are the voltage and pressure difference, respectively. The value of C (V Pa^{-1}) has been used in numerous studies to predict the magnitude of the voltage gradient for a given pressure gradient [e.g., *Wurmstich and Morgan*, 1994; *Revil et al*., 2007; *Saunders et al*., 2008; *Allègre et al*., 2010; *Vinogradov and Jackson*, 2011]. When there is more than one fluid occupying the pore space, a streaming current can be defined for each fluid phase and the total streaming current is the sum of the individual phase contributions. However, in many natural systems, water is the only fluid phase that transports electrical charge, so the electrical conductivity σ and coupling coefficient C become functions of water saturation [*Jackson*, 2008]:

$$j_s = -\sigma\sigma_r C C_r \nabla P_w \tag{4}$$

where σ and C are the electrical conductivity and coupling coefficient when the porous medium is fully water saturated ($S_w = 1$), and the relative electrical conductivity and streaming potential coupling coefficient are given by [*Guichet et al*., 2003; *Revil and Cerepi*, 2004]

$$C_r = C(S_w)/C(S_w = 1) \tag{5a}$$

$$\sigma_r = \sigma(S_w)/\sigma(S_w = 1) = I^{-1} \tag{5b}$$

where I is the so-called resistivity index. The saturation-dependent relative electrical conductivity σ_r (or resistivity index I) is often described using Archie's second law or variants thereof [*Dullien*, 1992]. However, the saturation dependence of the relative coupling coefficient C_r remains poorly understood.

A number of models have been published for the saturation dependence of C_r (summarized in Table 1) [e.g., *Wurmstich and Morgan*, 1994; *Perrier and Morat*, 2000; *Guichet et al*., 2003; *Darnet and Marquis*, 2004; *Revil and Cerepi*, 2004; *Linde et al*., 2007; *Jackson*, 2010; *Jougnot et al*., 2012]. *Wurmstich and Morgan* [1994] and *Darnet and Marquis* [2004] both predicted that C_r should increase with decreasing water saturation based on the assumption that the nonwetting phase is transported as bubbles. However, this assumption is not appropriate when both phases are continuously distributed throughout the pore space. *Guichet et al*. [2003] suggested that C_r varies linearly with water saturation. *Revil and Cerepi* [2004] developed a nonlinear relationship between C_r and S_w.

Titov et al. [2002] described the streaming current j_s (A m^{-2}) in terms of the streaming current charge density Q_s (C m^{-3})

$$j_s = Q_s q_w \tag{13}$$

where q_w is the Darcy velocity of the water. They attempted to relate the streaming charge density with the intrinsic hydraulic conductivity and concluded that the streaming charge density is not influenced by permeability. *Linde et al*. [2007] and *Revil et al*. [2007] later equated Q_s with the excess charge per unit pore volume in the diffuse layer (termed here Q_v) and argued that Q_v scales inversely with water saturation. This model for the saturation dependence of Q_s has been used to match experimental measurements of streaming potential

Table 1. Summary of Published Relationships for the Saturation Dependence of the Relative Coupling Coefficient

Authors	Expression	Equation #
Wurmstich and Morgan [1994][a]	$C_r(S_w) = \frac{(1-w)}{\sigma_r(S_w)}$	(6)
Perrier and Morat [2000]	$C_r(S_w) = \frac{k_{rw}(S_w)}{\sigma_r(S_w)}$	(7)
Guichet et al. [2003]	$C_r(S_w) = S_w$	(8)
Darnet and Marquis [2004]	$C_r(S_w) = \frac{1}{\sigma_r(S_w)}$	(9)
Revil and Cerepi [2004][b]	$C_r(S_w) = \frac{\beta_{(+)}\left(\sqrt{R^2+1}+R\right)+\beta_{(-)}\left(\sqrt{R^2+1}-R\right)}{\beta_{(+)}\left(\sqrt{R^2+1}+R_s\right)+\beta_{(-)}\left(\sqrt{R^2+1}-R_s\right)}$	(10)
Revil et al. [2007]	$C_r(S_w) = \frac{k_{rw}(S_w)}{S_w\sigma_r(S_w)}$	(11)
Jackson [2010]	$C_r(S_w) = \frac{k_{rw}(S_w)Q_{rs}(S_w)}{\sigma_r(S_w)}$	(12)

[a] w is the hydrodynamic resistance factor.
[b] R represents the excess of counter-ions in the pore water of the rock; β is the mobility of ions.

using a similar approach to the one proposed herein [*Linde et al.*, 2007]. However, *Allègre et al.* [2014] performed a succession of drainage and imbibition cycles in a sandpack and attempted to build a model of C_r (S_w) assuming the $1/S_w$ dependence of Q_r but was unable to obtain a satisfactory match. Moreover, simple pore-scale models that capture the distribution of fluids, electrical charge, and flow demonstrate that $Q_v \neq Q_s$ at partial saturation, because of the heterogeneous distribution of water within pores of different sizes and the nonuniform flow field within a given pore [*Jackson*, 2008; *Linde*, 2009; *Jackson*, 2010; *Jougnot et al.*, 2012, 2015]. *Jougnot et al.* [2012] used a bundle of capillary tubes model to calculate the saturation dependence of Q_s, iteratively adjusting the capillary size distribution to match experimentally measured water retention curves (their WR method) or relative permeability curves (their RP method). Their approach was applied successfully by *Jougnot et al.* [2015] to model field measurements of streaming potential in an agricultural test site. However, a bundle of capillary tubes model is too simple to capture the complex pore space topology of most geologic porous media.

A number of experimental measurements of streaming potential during multiphase flow have also been reported (Figure 1). *Guichet et al.* [2003] measured the streaming potential during drainage under gas in a water-wet sandpack and reported a monotonic decrease in relative coupling coefficient (Figure 1a); however, in similar experiments, *Allègre et al.* [2010] obtained strongly nonmonotonic behavior, with the relative coupling coefficient increasing by some 2 orders of magnitude before decreasing with decreasing water saturation (Figure 1b). *Revil et al.* [2007] also reported a monotonic behavior of relative coupling coefficient in dolomite core samples, but, as pointed out by *Allègre et al.* [2011], they calculated C_r based on a value of C ($S_w = 1$) that was extrapolated from the data obtained at partial saturation. When their data are rescaled to the value of C ($S_w = 1$) reported by *Revil and Cerepi* [2004] for experiments on the same samples, C_r again exhibits nonmonotonic behavior and exceeds the value at saturation (Figure 1a; compare open and closed triangles, noting the closed triangles plot against the right-hand axis).

A common feature of the studies reported above is that they observed zero streaming potential at the irreducible water saturation when water flow ceased. In contrast to these studies, *Moore et al.* [2004] and *Vinogradov and Jackson* [2011] observed a nonzero streaming potential (and, hence, coupling coefficient) at the irreducible water saturation. They measured the streaming potential during unsteady state displacements in sandstone core samples, in which a nonaqueous, nonwetting phase (gas, oil, or supercritical CO_2) was injected into an initially water-saturated sample during drainage, and then water was injected into the same sample at the irreducible water saturation during imbibition. *Vinogradov and Jackson* [2011] suggested that flow of the nonwetting phase at the irreducible water saturation drags with it small volumes

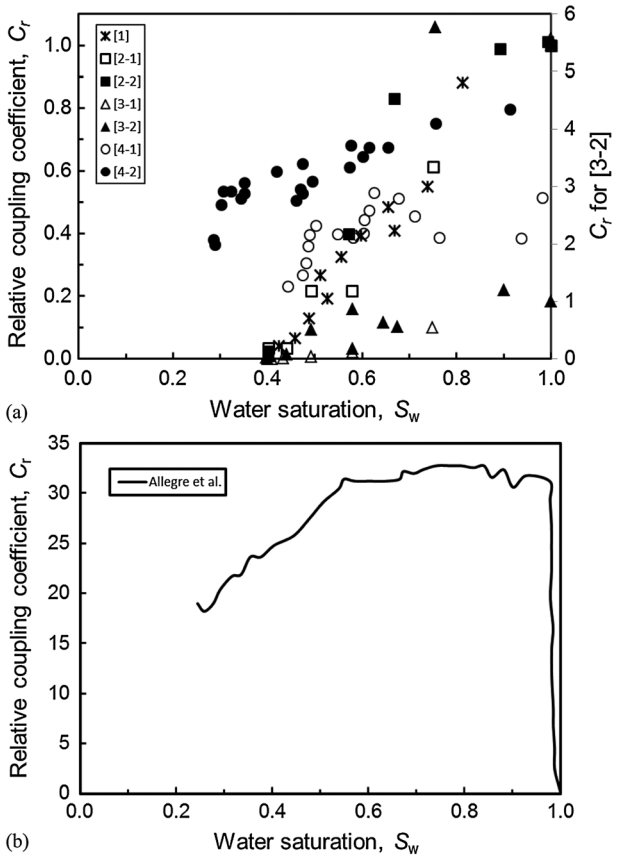

Figure 1. Experimental studies of the saturation dependence of the relative streaming potential coupling coefficient during drainage: (a) [1] data from *Guichet et al*. [2003]; [2-1] and [2-2] data from *Revil and Cerepi* [2004] for samples E39 and E3, respectively; [3-1] data from *Revil et al*. [2007] with extrapolated $C(S_w = 1)$; [3-2] data from *Revil et al*. [2007] with C_r calculated using $C(S_w = 1)$ reported by *Revil and Cerepi* [2004]; [4-1] and [4-2] data from *Vinogradov and Jackson* [2011] for samples Stainton and St. Bees, respectively. (b) The relative coupling coefficient obtained by *Allègre et al*. [2010] between their electrodes 6 and 7 in experiment #1.

of charge-rich water, giving rise to a streaming current and hence a nonzero coupling coefficient. Capillary desaturation experiments such as those conducted by *Revil and Cerepi* [2004], *Revil et al*. [2007], and *Allègre et al*. [2010] will always result in zero streaming potential at the irreducible saturation, because there is no flow of either the wetting or nonwetting phases.

Unsteady state displacements such as those conducted by *Moore et al*. [2004] and *Vinogradov and Jackson* [2011] are widely used to measure multiphase transport properties such as relative permeability, which cannot be obtained directly from the capillary desaturation experiments more typically used to measure multiphase SP. However, in such displacements, the water saturation in the sample is not uniform except at the initial (fully water saturated) condition, the irreducible water saturation, and the residual nonwetting phase saturation. Consequently, the permeability, streaming potential, and electrical conductivity measured across the sample are apparent values. These measured data cannot be used to interpret or model multiphase flows where it is assumed that the saturation is uniform within a representative elementary volume (REV) [e.g., *Dullien*, 1992]. Instead, it is necessary to develop and apply methods to interpret data from unsteady state displacement experiments to determine values of the parameters of interest within a REV. An alternative to unsteady state measurements is to use the steady state method where both phases flow at constant rate through the porous medium of interest, but steady state measurements are considerably more complex and time consuming to obtain [*Dullien*, 1992] and no such measurements of streaming potential at partial saturation have been reported to date.

Sigmund and McCaffery [1979] proposed a method to interpret the saturation dependence of relative permeability in unsteady state displacements, in which they used numerical simulation to fit Corey-type relative permeability functions to the observed flow rate and pressure data. In this paper, we develop a similar approach to interpret unsteady state measurements of relative permeability (k_r), electrical conductivity (σ), the streaming potential coupling coefficient (C), and the streaming current charge density (Q_s). The approach can be used to interpret any measurements of streaming potential obtained in unsteady state displacements.

We apply the method to the experimental data obtained during drainage and imbibition using two sandstone samples by *Vinogradov and Jackson* [2011] and report new data for Q_s in natural geologic porous media. Few studies have interpreted Q_s from experimental data, and the saturation dependence of Q_s in real geologic porous media is still poorly understood. We find that Q_s increases with decreasing S_w but is not

given by $1/S_w$ as is often assumed. The variation in Q_s with S_w is very similar for a given sample and a given drainage or imbibition process, and the difference between samples is less than the difference between drainage and imbibition. Based on the results, we propose a simple model for the saturation dependence of Q_s which can be used, along with modeled or measured values of relative permeability (k_r) and electrical conductivity (σ_r) to predict the complex behavior of C_r observed in experiments. The results and models can be used to assist in the interpretation SP and SE measurements obtained from partially saturated subsurface settings.

2. Methodology

To determine the saturation dependence of the coupling coefficient within a REV requires the values of ΔP, ΔU, and S_w across each REV. To determine the streaming current charge density Q_s, it also requires the value of σ. These parameters were obtained here using numerical modeling to predict values across a cylindrical rock core sample ($-C$, $-S_w$, and $-\sigma$) and optimization to minimize the difference between predicted and observed values. A finite difference approach was used to discretize the governing equations, assuming that mass and current flow can be modeled in one dimension (1-D) along the core sample. The numerical model divided the core sample into 100 equally sized grid blocks, each with a volume of approximately 1×10^{-6} m^3. This is a similar volume to that used in pore network models of sandstones, which typically contain a few thousand pores and throats and are assumed to represent a REV [e.g., *Blunt et al*., 2002]. Hence, we consider each grid block to be a REV with uniform saturation and identical material properties, although we recognize that the REV may be smaller and may also vary with saturation [*Doussan et al*., 2002; *Joekar-Niasar and Hassanizadeh*, 2011].

The numerical modeling and optimization approach was subdivided into three steps. In step 1 (the "hydraulic optimization"), we used a commercial package [*Schlumberger*, 2013] to solve Darcy's law (equation (1)) for each phase (neglecting the electrokinetic coupling, in common with numerous similar studies) [see, e.g., *Saunders et al*., 2006; *Gulamali et al*., 2011] and the continuity equation for mass, to determine the saturation-dependent relative permeability and capillary pressure functions applied to each REV that best match the observed pressure drop and effluent phase flow rates over the duration of the experiment. This allowed us to predict the saturation in each REV at a given time.

In step 2 (the "conductivity optimization"), we used a simple harmonic average of the electrical conductivity in each REV at a given time, to determine the saturation-dependent relative electrical conductivity function in each REV that best matches the experimentally measured electrical conductivity of the partially saturated core. This allowed us to predict the electrical conductivity in each REV at a given time. Finally, in step 3 (the "electrokinetic optimization"), we used an in-house finite difference code to solve the modified Ohm's law (equation (2)), plus the continuity equation for charge, to determine the saturation-dependent relative coupling coefficient function in each REV that best matches the experimentally measured voltage drop across the partially saturated core sample at a given time. This final step yielded the desired objective: the relative coupling coefficient as a function of saturation within an REV.

Dimensions, permeability, and porosity of the core samples in the numerical model were consistent with those used in the unsteady state displacements described by *Vinogradov and Jackson* [2011]. They measured the pressure difference (ΔP), the streaming potential (ΔU), the electrical conductivity ($-\sigma$), and the average water saturation ($-S_w$) across two intact, water-wet, sandstone core samples during drainage and imbibition of undecane and water (a simple 0.01 *M* solution of NaCl in de-ionized water). The hydraulic optimization model also includes the inlet fluid reservoir and connecting flow line (Figure 2). We used Darcy's law in the same pseudo 1-D model to describe flow within the reservoir and flow line, with the permeability adjusted to yield the appropriate flow resistance for a cylindrical tube of the same diameter. In a preliminary optimization step, the compressibility of the reservoir and flow line was adjusted to match the gradual buildup of pressure measured in the experiments at the sample inlet when the pump was switched on.

The initial and boundary conditions for the hydraulic models of drainage and imbibition matched the laboratory experiments. During drainage, the initial conditions were a uniform initial water saturation of 1 and atmospheric pressure; the boundary conditions were a fixed flow rate of undecane into the inlet fluid reservoir, determined by the flow rates applied during the experiments, and atmospheric pressure at the outlet

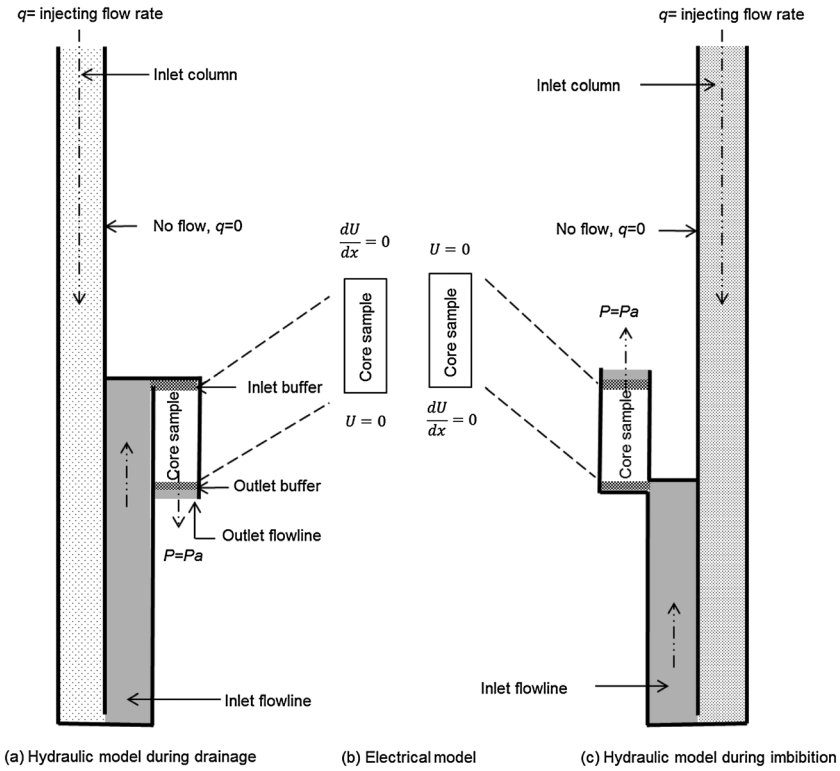

Figure 2. Schematic of the 1-D numerical models used to interpret hydraulic and electrical properties measured experimentally: (a) Hydraulic model during drainage. Dashed arrows represent flow within the hydraulic model. Black bold lines represent no-flow boundaries. (b) Electrical model during both drainage and imbibition to interpret the measured apparent electrical conductivity and coupling coefficient. (c) Hydraulic model during imbibition, in which the inlet flow line was modified by connecting to the base of the core sample.

from the core (Figure 2a). During imbibition, the initial conditions for the hydraulic model were uniform initial water saturation at the end of drainage ($S_w = S_{wir}$) and atmospheric pressure; the boundary conditions were a fixed water flow rate into the inlet fluid reservoir, determined by the flow rates applied during the experiments, and atmospheric pressure at the outlet from the core (Figure 2c).

The electrical model, used to optimize the electrical conductivity and electrokinetic properties, included only the core sample and was treated as a postprocessing step using the outputs of pressure and saturation from the hydraulic model at a given time. The boundary conditions for the conductivity optimization were a constant (arbitrary) current through the inlet and outlet faces; the boundary conditions for the electrokinetic optimization were dU/dx = 0 at the inlet flow boundary and U = 0 at the outlet flow boundary. This reproduced the earthed electrode used in the experiments (Figure 2b) [*Vinogradov and Jackson*, 2011].

2.1. Parameter Optimization During Drainage

The hydraulic optimization was to determine the relative permeability (k_r) and capillary pressure (P_c) (Pa) in each REV that yield the best match to the measured experimental data using the hydraulic numerical model. Following the approach of *Sigmund and McCaffery* [1979], we assumed the following drainage functions for k_r and P_c:

$$k_{rw} = S_{wn}{}^{\alpha} \tag{14}$$

$$k_{ro} = \frac{k(S_{wir})}{k(S_w = 1)}(1 - S_{wn})^{\beta} \tag{15}$$

$$P_c = \begin{cases} A \cdot P_{ce}\left(S_{wn}^{-\frac{1}{\lambda}} - 1\right) & (S_{wn} \neq 0) \\ A \cdot P_{ce} & (S_{wn} = 0) \end{cases} \tag{16}$$

where S_{wn} is the normalized water saturation given by

$$S_{wn} = \frac{S_w - S_{wir}}{1 - S_{wir} - S_{nwr}} \tag{17}$$

S_{wir} is the irreducible water saturation after drainage and S_{nwr} is the residual nonwetting phase saturation after imbibition. The capillary entry pressure P_{ce} (Pa) is estimated using the Leverett *J*-function [*Leverett*, 1942]

$$P_{ce} = \gamma(k/\varnothing)^{-0.5} \tag{18}$$

where γ is the air brine surface tension (estimated at 30 mN m^{-1}), ϕ is the porosity (0.19 for St. Bees and 0.13 for Stainton as reported in Table 1 from *Vinogradov and Jackson* [2011]), and k is the absolute permeability (20 mD for St. Bees and 1.634 mD for Stainton), yielding $P_{ce} = 9.334 \times 10^4$ Pa and $P_{ce} = 2.694 \times 10^5$ Pa for St. Bees and Stainton, respectively.

The optimization problem for drainage (in which $S_{nwr} = 0$) is then reduced to one of finding the values of S_{wir}, α, β, λ, and A that yield simulated pressure and phase flow rates that most closely match the experimentally measured values. Values of S_{wir} were constrained to lie within the experimentally measured range ($S_{wir} = 0.29 \pm 0.08$ for the St. Bees sample investigated by *Vinogradov and Jackson* [2011] and $S_{wir} = 0.44 \pm 0.08$ for the Stainton sample investigated by *Vinogradov and Jackson* [2011]). The problem to match simulated (subscript sim) pressure drop across the sample (ΔP), total volume of produced fluid (V_f), and water fractional flow at the outlet (F_w) with observed (subscript obs) values becomes an optimization of a least squares objective function:

$$f_1 = \sum\left(\frac{\Delta P_{obs} - \Delta P_{sim}}{\delta_P}\right)^2 + \sum\left(\frac{V_{f_{obs}} - V_{f_{sim}}}{\delta_V}\right)^2 + \sum\left(\frac{F_{w_{obs}} - F_{w_{sim}}}{\delta_F}\right)^2 \tag{19}$$

We weighted each difference with the experimental uncertainties δ_P, δ_V, and δ_F in equation (19) to make the quality of match of ΔP, V_f, or F_w dimensionless and minimized the objective function (f_1) using constrained sequential quadratic programming (SQP) nonlinear optimization [see, e.g., *Nocedal and Wright*, 2006] implemented in Matlab [*MATLAB*, 2012]. We used SQP in this study because it has been shown to have high efficiency, accuracy, and success over a large number of test problems [e.g., *Schittkowski*, 1985]. Given the highly nonlinear nature of the governing equations (coupled through, for example, the saturation-dependent relative permeability and capillary pressure functions [*Dullien*, 1992]) the optimization solutions are likely to be nonunique and the optimization may find local rather than global minima. In an attempt to account for this, we chose the best eight sets of optimized parameters with a similar quality of match (the minimum value of f_1 + 10% variation) to take into the next step of the optimization (Figure 3), rather than a single set of parameters.

In the conductivity optimization, we used the simulated values of water saturation to determine the electrical conductivity of each REV. To do this requires the saturation-dependent relative electrical conductivity (σ_r) in each REV. We assumed a modified Archie's law which accounts for surface electrical conductivity [e.g., *Clavier et al*., 1984; *Revil and Glover*, 1998; *Glover et al*., 2000]:

$$\sigma = a_1 \cdot S_w^n + a_2 \tag{20}$$

in which n corresponds to the saturation exponent, a_1 corresponds to the bulk electrical conductivity when the rock is fully water saturated, and a_2 corresponds to the surface electrical conductivity, which is assumed to be independent of saturation because the samples are strongly water-wet so water forms a continuous film along the mineral surfaces at partial saturation [*Hearst and Nelson*, 1985]. We constrain

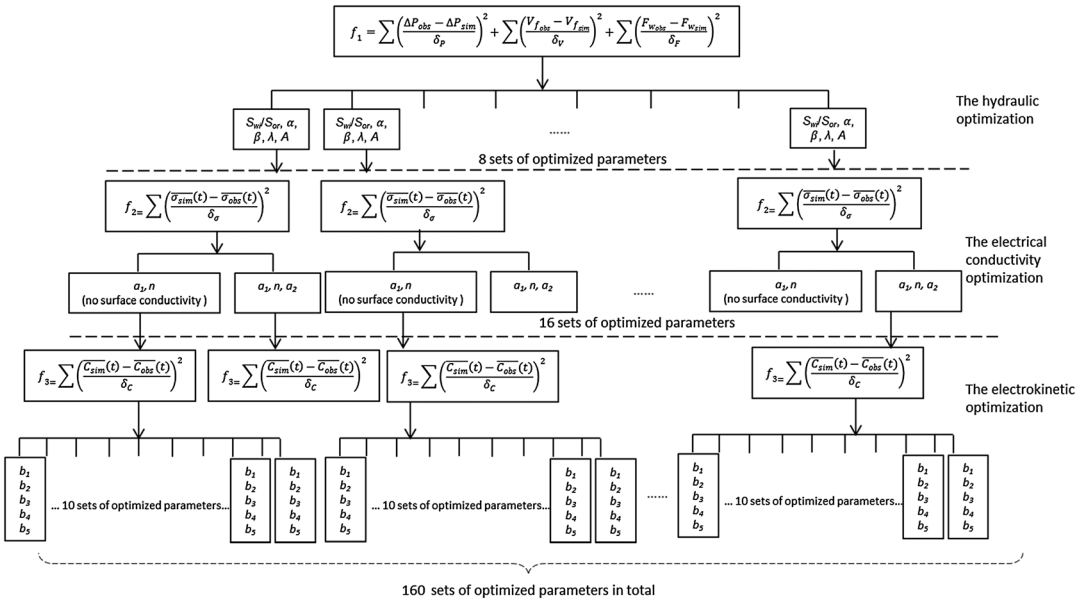

Figure 3. Flowchart showing the three optimization steps during drainage/imbibition: the hydraulic optimization, the electrical conductivity optimization, and the electrokinetic optimization.

$a_1 + a_2 = \sigma_{obs}(S_w = 1)$ because the simulated electrical conductivity must equal the observed electrical conductivity when the rock is fully water saturated. The objective function f_2 was a the sum of the weighted squared difference between observed and simulated sample electrical conductivity at a given time t

$$f_{2=} \sum \left(\frac{\overline{\sigma_{sim}}(t) - \overline{\sigma_{obs}}(t)}{\delta_\sigma} \right)^2 \tag{21}$$

where δ_σ is the experimental uncertainty of electrical conductivity. For each of the eight sets of optimized hydraulic parameters obtained in the previous step, we identified the values of a_1, n, and a_2, and a_1 and n with $a_2 = 0$, that minimized the objective function (equation (21)). Thus, 16 sets of optimized parameters were taken into the final optimization step (Figure 3).

In the final step (the electrokinetic optimization) we used the simulated values of pressure, water saturation, and electrical conductivity obtained using the optimized parameter sets in the previous steps to determine the streaming potential drop across each REV. The sum of these potential drops yields the total streaming potential measured across the sample. To do this requires the saturation-dependent relative streaming potential coupling coefficient (C_r) in each REV. Since there is no general model to describe the saturation dependence of C_r and experimental data to date has suggested complex, nonmonotonic behavior, high-order functions have been tested to match the complex behavior of C measured in experiments. We varied the order of the polynomial approximation in a preliminary step and found that the quality of match to the experimental data did not significantly increase above order 4 but was significantly better than order 3, so we used an order 4 polynomial function given by

$$C_r = b_1 \cdot {S_{wn}}^4 + b_2 \cdot {S_{wn}}^3 + b_3 \cdot {S_{wn}}^2 + b_4 \cdot S_{wn} + b_5 \tag{22}$$

where b_1, b_2, b_3, b_4, and b_5 are fitting parameters to be adjusted in the optimization. The objective function f_3 was

$$f_3 = \sum \left(\frac{\overline{C_{sim}}(t) - \overline{C_{obs}}(t)}{\delta_C} \right)^2 \tag{23}$$

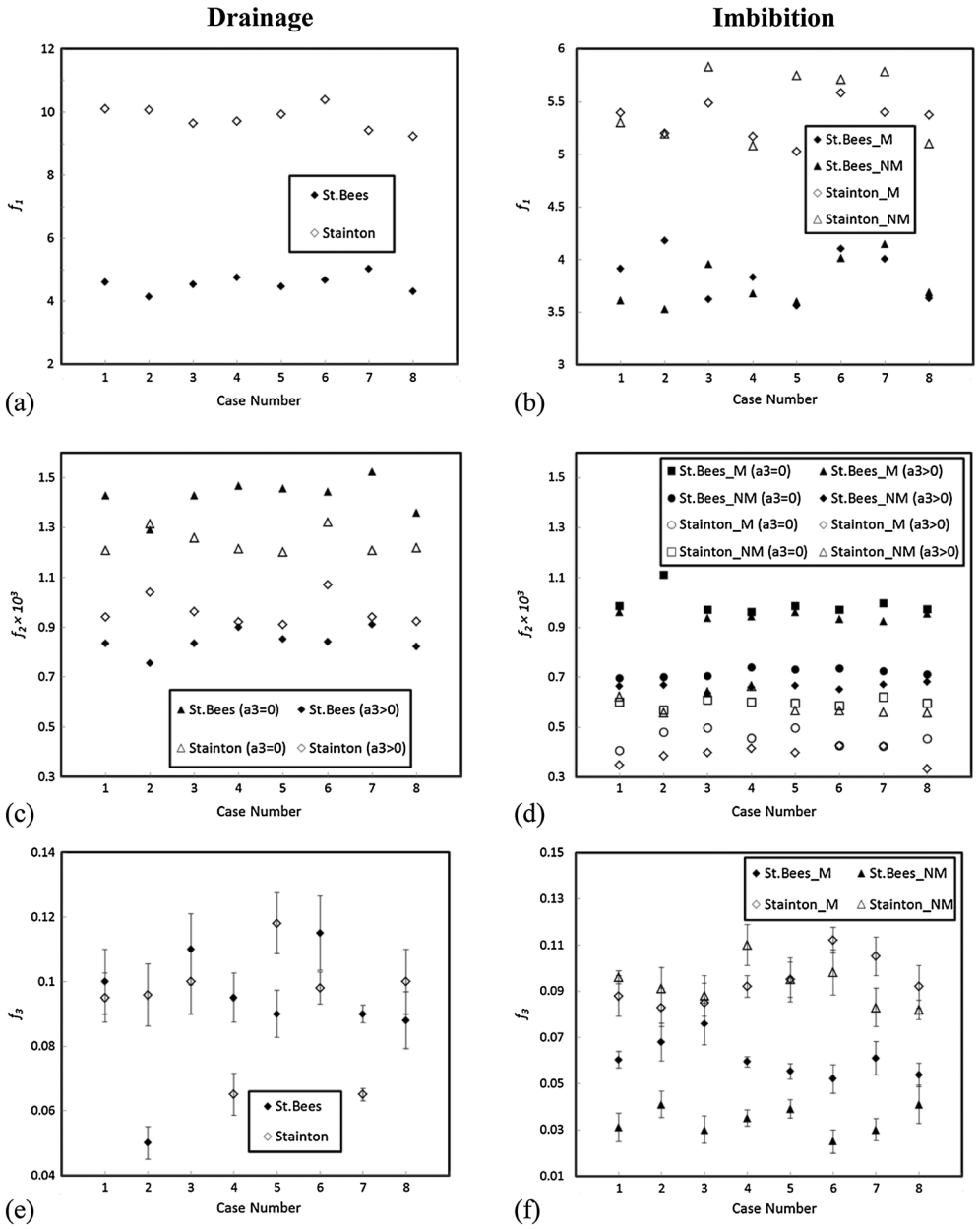

Figure 4. Objective function values in hydraulic (f_1), electrical conductivity (f_2), and electrokinetic (f_3) optimizations: (a, c, e) objective function values from St. Bees (solid points) and Stainton (hollow points) samples during drainage; (b, d, f) objective function values in St. Bees (solid points) and Stainton (hollow points) samples during imbibition. Case number corresponds to the eight sets of optimized parameters obtained in the hydraulic optimization during drainage. We selected two initial conditions for imbibition from the ensemble obtained at the end of the drainage optimization (one showing monotonic behavior of C_r denoted M and the other showing nonmonotonic behavior denoted NM). The error bars shown in Figures 4e and 4f represent the spread in f_3 that yield a similar quality of match after the electrokinetic optimization.

where δ_C represents the measured uncertainty of the streaming potential coupling coefficient. Although we use an arbitrary polynomial function to describe C_r, we recognize that the streaming charge density in a water-wet rock must increase with decreasing water saturation, because the mobile electric charges are located within the wetting water layers and the nonwetting phase occupies the pore centers [*Linde et al.*, 2007; *Revil et al.*, 2007; *Jackson*, 2010]. We used this condition to reject some solutions for C_r obtained from the optimization; only C_r solutions in which Q_{rs} (calculated using equation (13) in Table 1) increased monotonically were allowed, although there was no constraint placed directly on the optimization. In

some cases, we added a constraint to the optimization that forced C_r (S_{wir}) = 0 in each REV, to determine whether this influenced the solutions obtained. For each of the 16 sets of optimized parameters obtained from the previous steps, we chose the 10 sets of optimized electrokinetic parameters b with a similar quality of match (the minimum value of f_3 + 10% variation). Thus, the drainage optimization finished with 160 sets of optimized parameters b that yield 160 possible functional relationships for the relative streaming potential coupling coefficient for each sample (Figure 3).

2.2. Parameter Optimization During Imbibition

The optimization approach during imbibition was very similar to that used during drainage, except that the relative permeability curve for water becomes

$$k_{rw} = \frac{k(1 - S_{nwr})}{k(S_w = 1)} S_{wn}{}^{\alpha} \tag{24}$$

With measured permeability $k(1 - S_{nwr})$ at irreducible water saturation. Moreover, there is no constraint on the electrical conductivity optimization ($a_1 + a_2 \neq \sigma_{obs}(S_{nwr})$ in equation (23)), because water saturation is less than 1 at the end of imbibition. Finally, the initial conditions for imbibition vary depending upon the optimization parameters chosen for drainage. We selected two different initial conditions for imbibition from the ensemble of optimized values at the end of drainage, one of which yielded a monotonic saturation dependence for C_r during drainage and the other of which yielded a nonmonotonic saturation dependence. The values of S_{nwr} during the hydraulic optimization were constrained to lie within the experimentally measured range (S_{nwr} = 0.088 ± 0.08 for the St. Bees sample and S_{nwr} = 0.095 ± 0.08 for the Stainton sample).

The imbibition optimization finished with 160 sets of optimized parameters b for each of the two selected starting conditions, thus yielding 320 possible functional relationships for the relative streaming potential coupling coefficient for each sample.

3. Results

3.1. Drainage Optimization

The objective function values (f_1, f_2, and f_3) obtained at the end of the hydraulic, electrical conductivity, and electrokinetic optimizations are plotted for both core samples during drainage (Figures 4a, 4c, and 4e) and imbibition (Figures 4b, 4d, and 4f). The case numbers listed on the horizontal axis correspond to the best eight sets of parameters obtained in the hydraulic optimization during drainage; since hundreds of values of f_3 were obtained during the electrokinetic optimization (see Figure 3) we represent the range of values using the error bars in Figures 4e and 4f. Moreover, since we selected two different initial conditions for imbibition from the ensemble obtained at the end of drainage, the number of optimized values is doubled.

Typical results from each step of the drainage optimization are shown in Figures 5–7, and the results are summarized in Table 2. Figure 5 shows typical results from the hydraulic optimization: there is a good match within experimental error to each of the measured parameters, and the two off-trend experimental data points around 15 h in Figure 5f most likely reflect the accumulation of air bubbles within the core sample. The spikes in pressure observed in Figures 5a and 5b reflect the experimental measurements of streaming potential.

Figure 6 shows typical results from the electrical conductivity optimization for cases without (Figures 6a and 6b) and with (Figures 6c and 6d) surface electrical conductivity (a_2 = 0 and $a_2 \neq 0$, respectively); the quality of match is not significantly affected by the value of a_2. Both samples exhibited a rapid initial decrease in measured relative electrical conductivity with decreasing water saturation, and this was very difficult to match using an Archie-type equation; indeed, despite numerous attempts, we failed to match the data within experimental error for water saturation values over the range 0.8–1, although the mismatch is small. Higher order polynomial relationships between σ_r and S_w were tested, and we also tried a three-stage Archie-type equation (in which the saturation exponent n in equation (20) had differing values for three different ranges of saturation), but the quality of fit was not significantly improved (f_2 values were reduced by less than 6×10^{-5}, which is small compared to the minimum values obtained; see Figure 4). Higher-order polynomial functions also yielded unphysical behavior. The shift in water saturation between observed

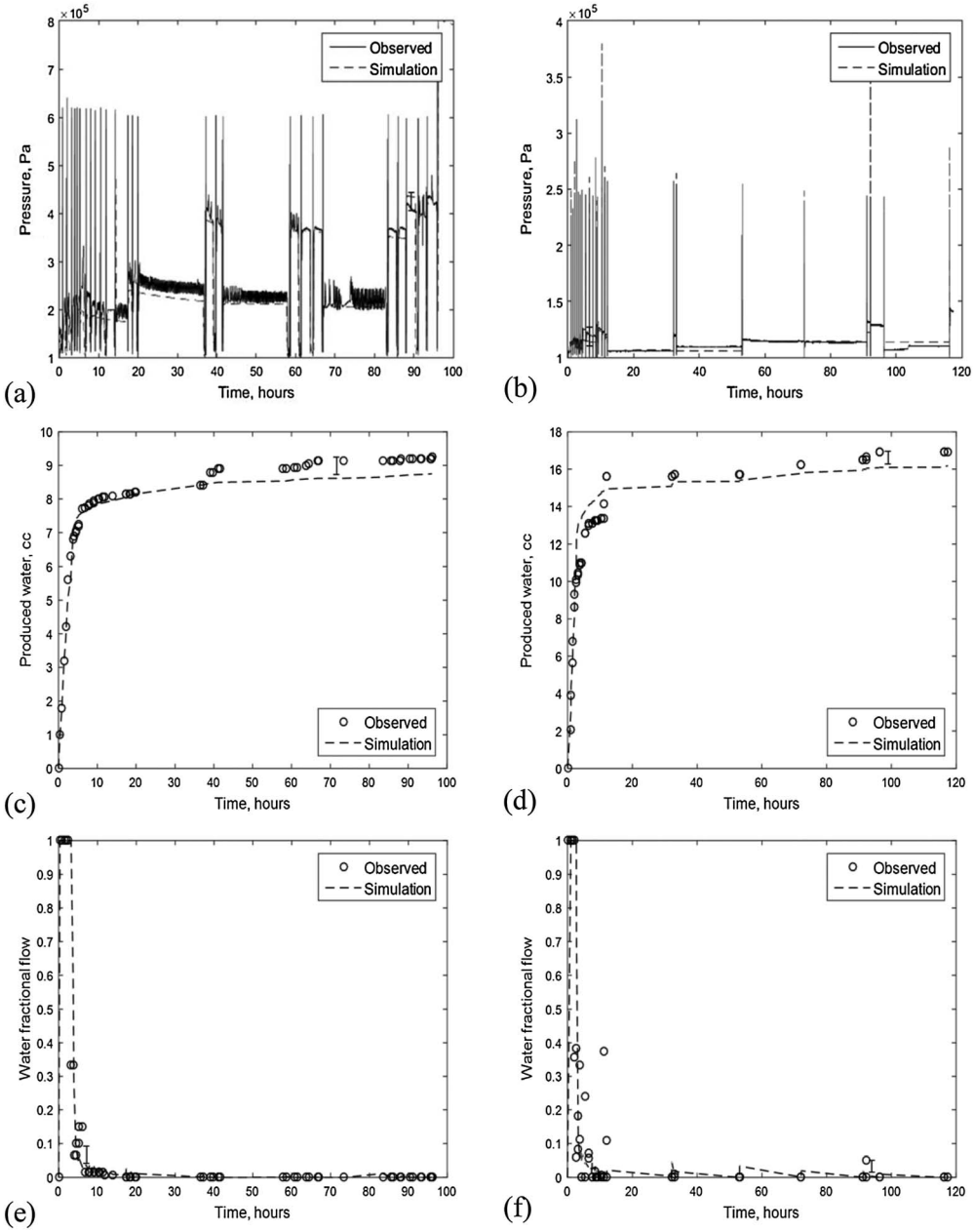

Figure 5. Typical results from the hydraulic optimization during drainage showing simulated (lines) and observed (points) data: pressure difference across (a) Stainton and (b) St. Bees samples; cumulative water production from the (c) Stainton and (d) St. Bees samples; water fractional flow at the outlet of the (e) Stainton and (f) St. Bees samples. Error bars denote the typical experimental error.

and simulated data is because we compared data at the same time step, rather than at the same saturation, as discussed above.

Figure 7 shows typical results from the electrokinetic optimization, which yielded both monotonic and nonmonotonic relationships between C_r and S_w with similar qualities of fit to the experimental data. Figure 7 shows examples of each relationship type compared to the measured data. The Stainton sample showed strongly nonmonotonic behavior at high water saturation, and it proved to be very difficult to match the initially rapid decrease in relative coupling coefficient with decreasing water saturation despite the use of a high-order polynomial, although the nonmonotonic behavior was captured. As before, the shift in water saturation between observed and simulated data is because we compared data at the same time step rather than at the

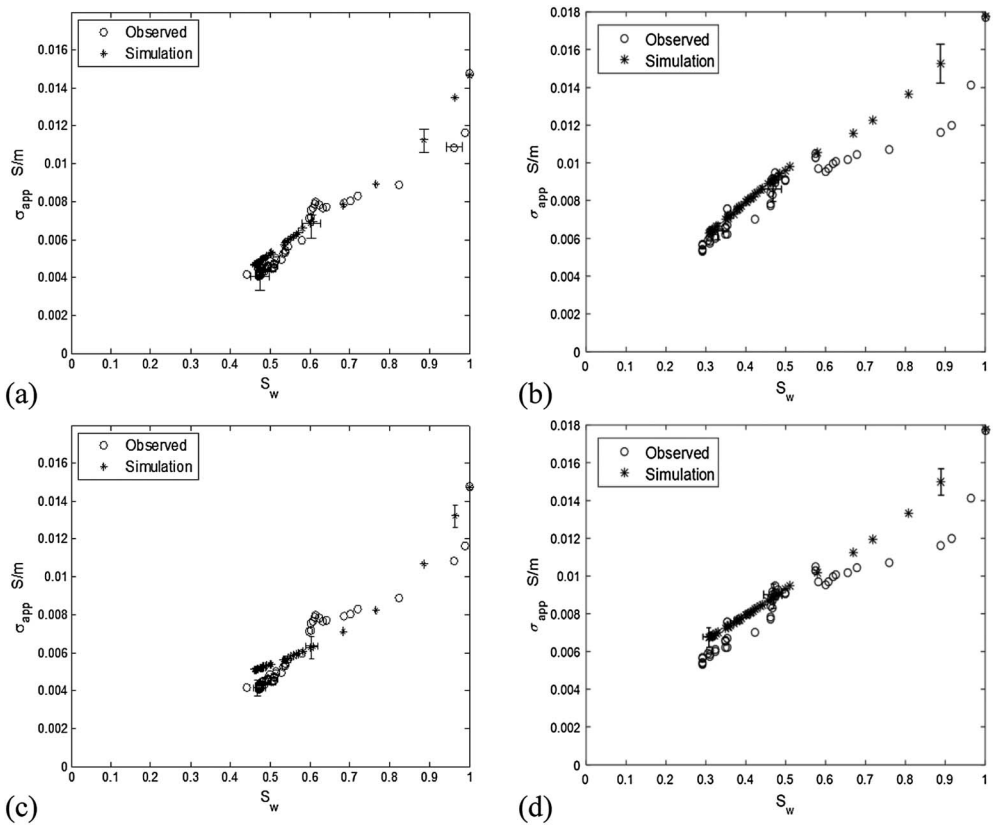

Figure 6. Typical results from the electrical conductivity optimization during drainage for (a, c) Stainton and (b, d) St. Bees during drainage: selected optimization results using Archie's law ($a_2 = 0$) (Figures 6a and 6b); selected optimization results using modified Archie's law with nonzero a_2 (Figures 6c and 6d). The error bar denotes the typical experimental error.

same saturation. The uncertainty in S_w is shown in Figures 6 and 7 and arises from the relatively low (±0.1 mL) precision in measuring the volume of produced liquid. This uncertainty is cumulatively increased during drainage and imbibition [*Vinogradov and Jackson*, 2011].

3.1.1. Imbibition Optimization

Typical results from each step of the imbibition optimization are shown in Figures 8–10, and the corresponding values are summarized in Table 3. Figure 8 shows typical results from the hydraulic optimization; there is a generally good match within experimental error to each of the measured parameters,

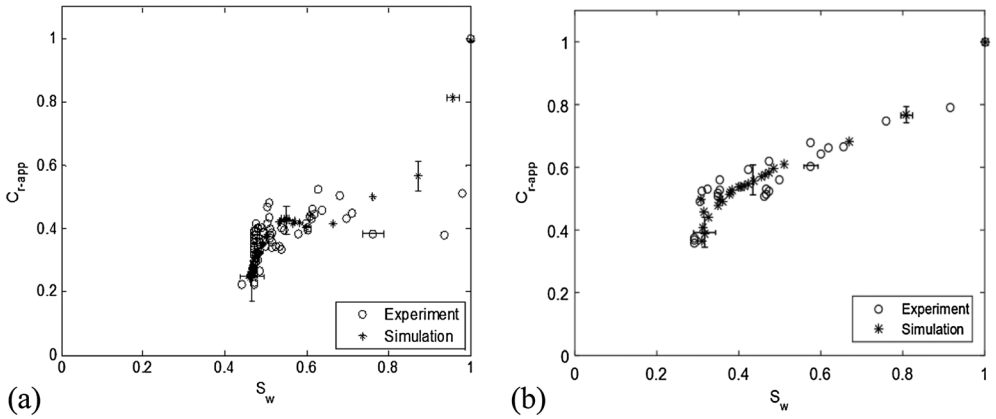

Figure 7. Typical results from the electrokinetic optimization during drainage for (a) Stainton and (b) St. Bees. The error bar denotes the typical experimental error.

Table 2. Optimized Values of Fitting Parameters During Drainage Shown in Figures 5–7

Values for Figures (5–7)	Sample	α	β	A	λ	S_{wir}
Hydraulic optimization	Stainton	3.721	2.316	0.102	9.321	0.374
	St. Bees	3.544	2.475	0.0433	6.001	0.238
		a_1 (S/m)		n	a_2 (S/m)	
Electrical conductivity optimization	Stainton	0.015		1.461	-	
		0.011		3.523	0.004	
	St. Bees	0.018		0.874	-	
		0.014		1.363	0.004	
		b_1	b_2	b_3	b_4	b_5
Electrokinetic optimization	Stainton	−6.274	16.089	−12.918	3.401	0.147
	St. Bees	−1.740	2.431	−0.544	0.389	0.448

although we were unable to obtain a good match to the late oil production (after 40 h) observed in the St. Bees sample (Figure 8d). The late increase in oil recovery is inconsistent with the well-established behavior of such immiscible displacements and is most likely an experimental artifact, possibly caused by the presence of air bubbles within the core sample. There may be microbubbles of oil trapped in the flow lines and extra oil was produced as a single slug when drops joined together. The spikes in pressure observed in Figures 8a and 8b reflect the Pressure Ramping (PR) measurements of streaming potential. The one off-trend experimental data point around 21 h in Figure 8f most likely reflects the accumulation of air bubbles within the core sample.

Figure 9 shows typical results from the electrical conductivity optimization for cases without (Figures 9a and 9b) and with (Figures 9c and 9d) surface electrical conductivity ($a_2 = 0$ and $a_2 \neq 0$, respectively); the quality of match is not significantly affected by the value of a_2. St. Bees exhibited a rapid initial increase in measured relative electrical conductivity with increasing water saturation at the start of imbibition, which was very difficult to match using an Archie-type equation despite numerous attempts. Higher-order polynomial functions and three-stage Archie-type equations were also tested during imbibition, but there was no significant improvement in the quality of fit (f_2 values were reduced by less than 5×10^{-5} which is small compared to the minimum values obtained; see Figure 5).

Figure 10 shows typical results from the electrokinetic optimization, which yielded both monotonic and non-monotonic relationships between C_r and S_w with similar qualities of fit to the experimental data; there is a good match within experimental uncertainties. As before, the shift in water saturation between observed and simulated data is because we compared data at the same time step rather than at the same saturation.

3.1.2. Interpretation of Optimization Results

Figures 11–13 show the optimized saturation dependence of the relative permeability, capillary pressure, electrical conductivity, and coupling coefficient across each REV; the spread in each (denoted by the dashed lines) reflects the range of parameter values selected at the end of each optimization step (Figure 3), and the solid line shows one specific example. Parameter values are summarized in Table 4.

As expected, relative permeability and capillary pressure exhibit monotonic but hysteretic behavior during drainage and imbibition (Figure 11). Hysteresis is observed because of the differing flow paths and contact angles during drainage and imbibition [e.g., *Brooks and Corey*, 1964; *Fenwick and Blunt*, 1998]. Hysteresis is also observed in the electrical conductivity, which can be related to changes in pore-scale fluid distribution caused by changes in saturation history [*Longeron et al.*, 1989; *Blunt et al.*, 2002]. Optimized values of the saturation exponent n are often lower than the range of 1.5–2.5 typically observed for sandstones [*Knight*, 1991]; many experimental and numerical studies have demonstrated that the saturation exponent n can be saturation-dependent, with smaller values observed at lower water saturation and values around 2 close to saturation [e.g., *Knight*, 1991; *Roberts and Lin*, 1997; *Suman and Knight*, 1997; *Knackstedt et al.*, 2007].

The relative coupling coefficient also demonstrates hysteretic behavior during drainage and imbibition for both samples. However, the most striking result is that the predicted relative coupling coefficient within an

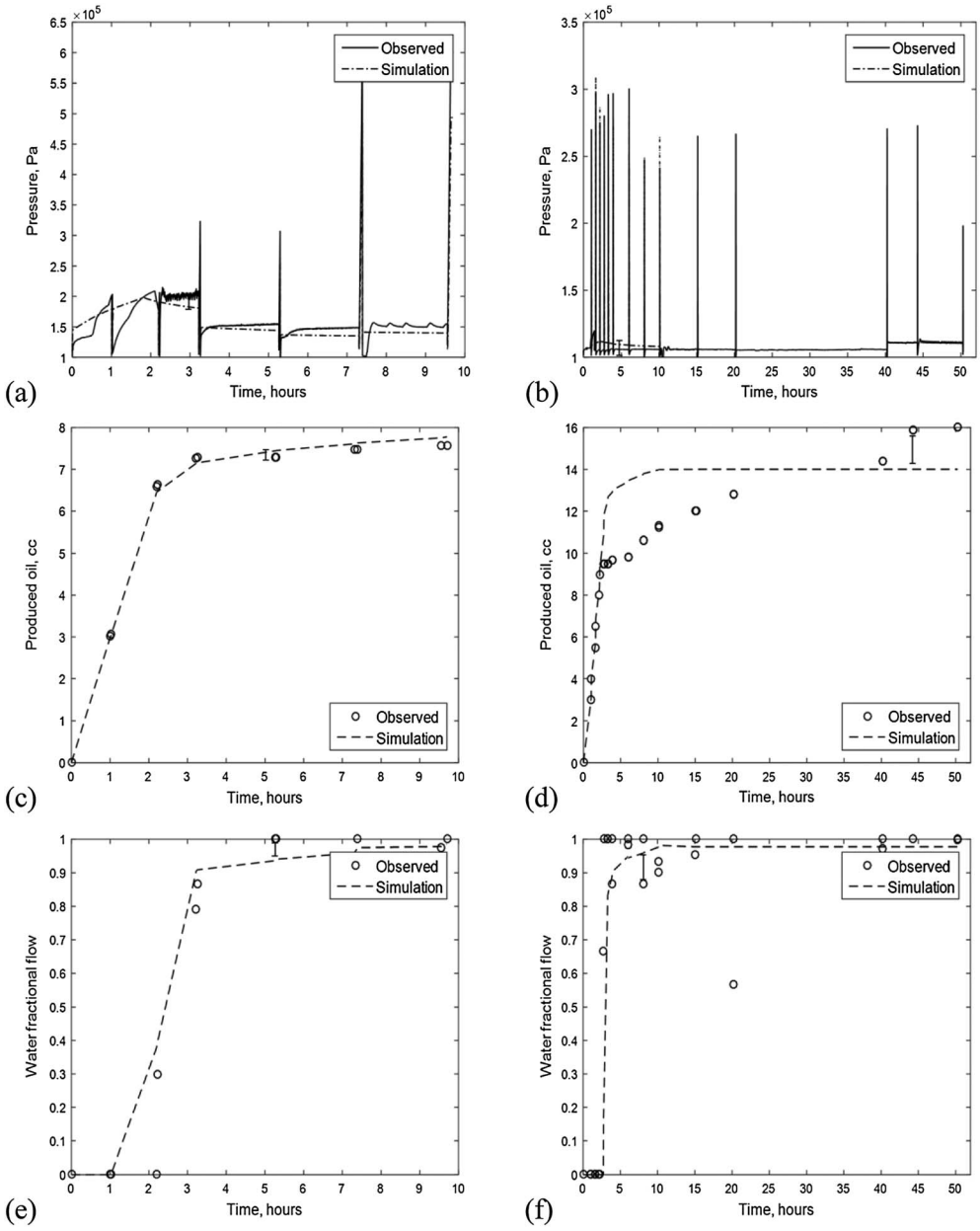

Figure 8. Typical results from the hydraulic optimization during imbibition showing simulated (lines) and observed (points) data: pressure difference across the (a) Stainton and (b) St. Bees samples; cumulative water production from the (c) Stainton and (d) St. Bees samples; water fractional flow at the outlet of the (e) Stainton and (f) St. Bees samples. Error bars denote the typical experimental error.

REV is consistent with experimental data and, during imbibition, can exceed the value observed at $S_w = 1$. The predictions also demonstrated strongly nonmonotonic behavior within an REV during drainage and imbibition. Moreover, the relative coupling coefficient at the REV may be 0 or nonzero at the irreducible water saturation but yield a similar quality of match to the apparent values measured across the core sample.

4. Discussion

4.1. Saturation Dependence of the Streaming Current Charge Density

Using the interpreted relative permeability, electrical conductivity, and streaming potential coupling coefficient functions, the saturation dependence of the relative streaming current charge density Q_r can be

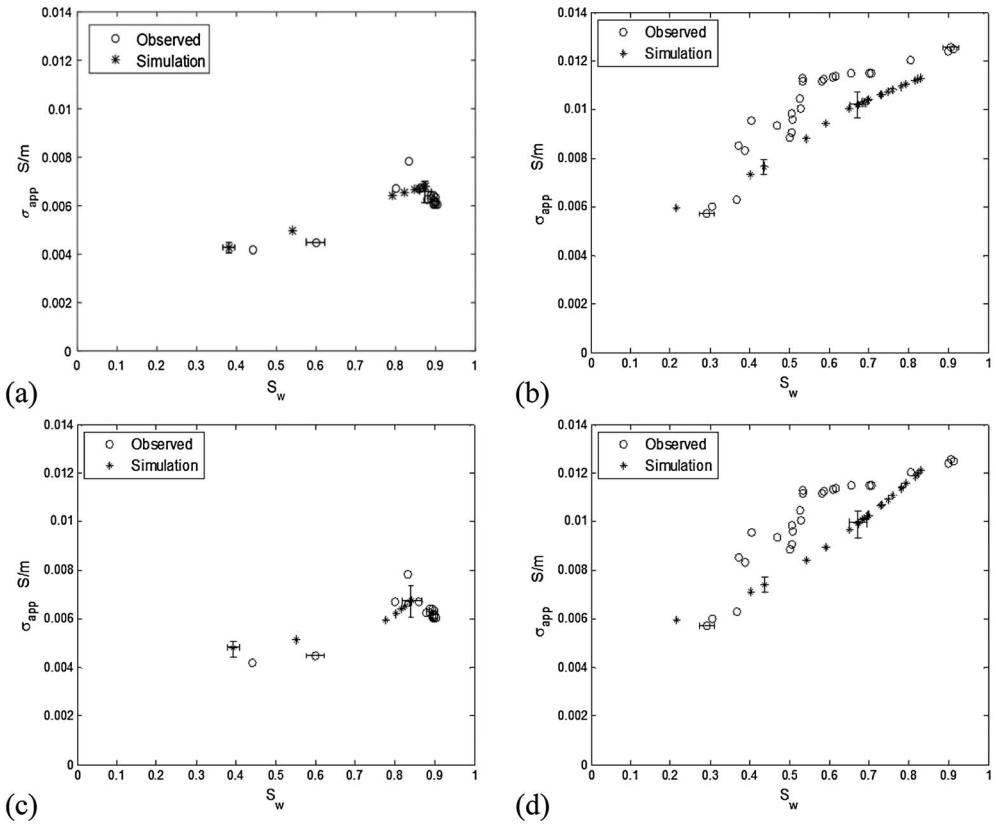

Figure 9. Typical results from the electrical conductivity optimization during imbibition for (a, c) Stainton and (b, d) St. Bees during drainage: selected optimization results using Archie's law ($a_2 = 0$) (Figures 9a and 9b); selected optimization results using modified Archie's law with nonzero a_2 (Figures 9c and 9d). The error bar denotes the typical experimental error.

calculated using equation (12) (Figure 14). The three-step optimization process adopted here yielded 160 ensembles of optimized relative permeability, electrical conductivity, and coupling coefficient for each sample during drainage and 320 ensembles during imbibition with, as discussed previously, a broad range of behaviors including both monotonic and nonmonotonic variations in the relative coupling coefficient. However, the variation in relative streaming charge density with saturation interpreted from these ensembles is very narrow for a given sample and a given drainage and imbibition process, and the difference between samples is less than the difference between drainage and imbibition; i.e., the spread of

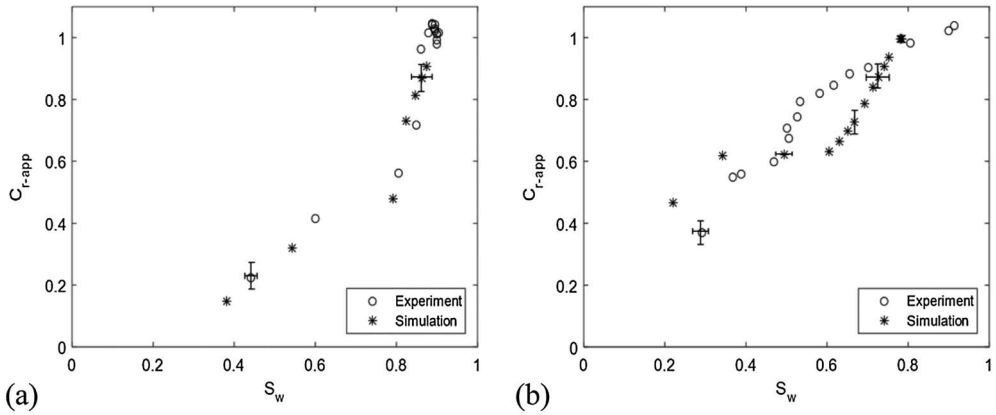

Figure 10. Typical results from the electrokinetic optimization during imbibition for (a) Stainton and (b) St. Bees. The error bar denotes the typical experimental error.

Table 3. Optimized Values of Fitting Parameters Shown in Figures 8–10 During Imbibition

Values for Figures 8–10	Sample	α	β	A	λ	S_{nwr}
Hydraulic optimization	Stainton	2.588	2.758	1.199E−5	65.598	0.038
	St. Bees	2.000	3.005	3.269E−5	194.17	0.168
		a_1 (S/m)		a_2 (S/m)	n	
Electrical conductivity optimization	Stainton	0.007		0.557	-	
		0.006		6.463	0.004	
	St. Bees	0.013		0.540	-	
		0.012		2.166	0.005	
		b_1	b_2	b_3	b_4	b_5
Electrokinetic optimization	Stainton	−27.637	62.379	−45.078	11.149	0.147
	St. Bees	−18.135	41.633	−30.295	7.348	0.465

Q_r curves is more similar for the two samples during drainage or imbibition than it is for a given sample for drainage and imbibition.

We model the relative streaming current charge density during drainage and imbibition using a power law function given by

$$Q_r\left(S_{wn}\right) = pS_{wn}^{-q} + r \tag{25}$$

where p, q, and r for a given sample and displacement are determined by curve fitting to the mean values of Q_r (S_{wn}) at each value of water saturation; $R^2 \geq 0.99999$ for all samples and displacements reported

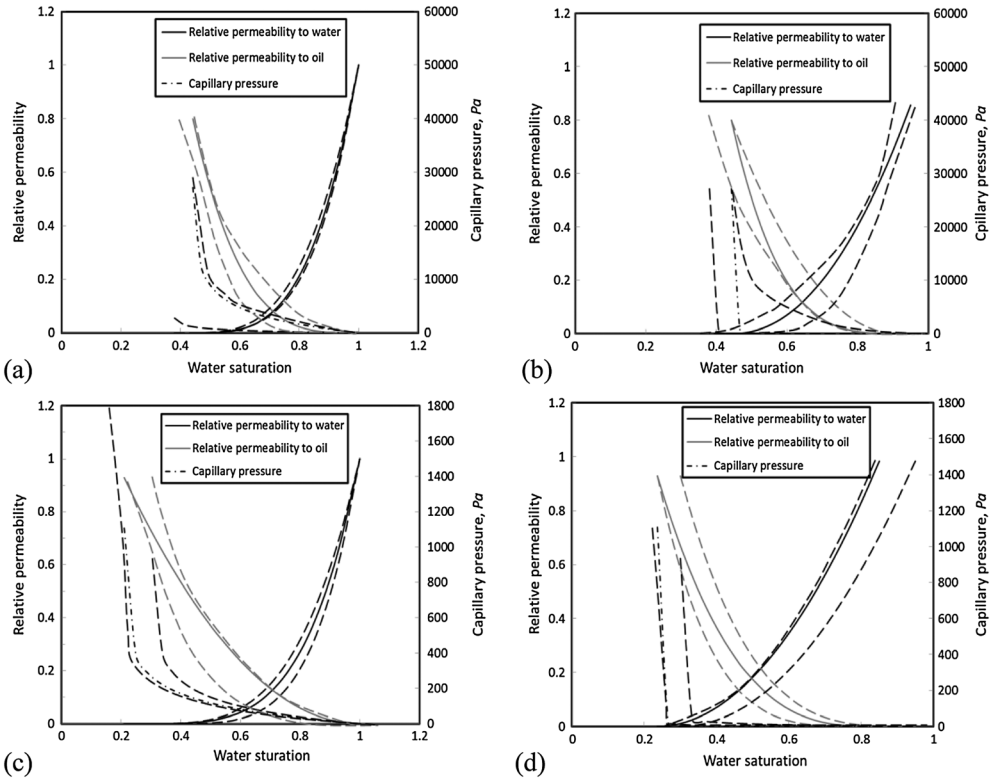

Figure 11. Summary results from the hydraulic optimization showing simulated data (solid and dash-dotted lines) and variations (dash lines): relative permeability and capillary pressure of the Stainton sample during (a) drainage and (b) imbibition; relative permeability and capillary pressure of the St. Bees sample during (c) drainage and (d) imbibition.

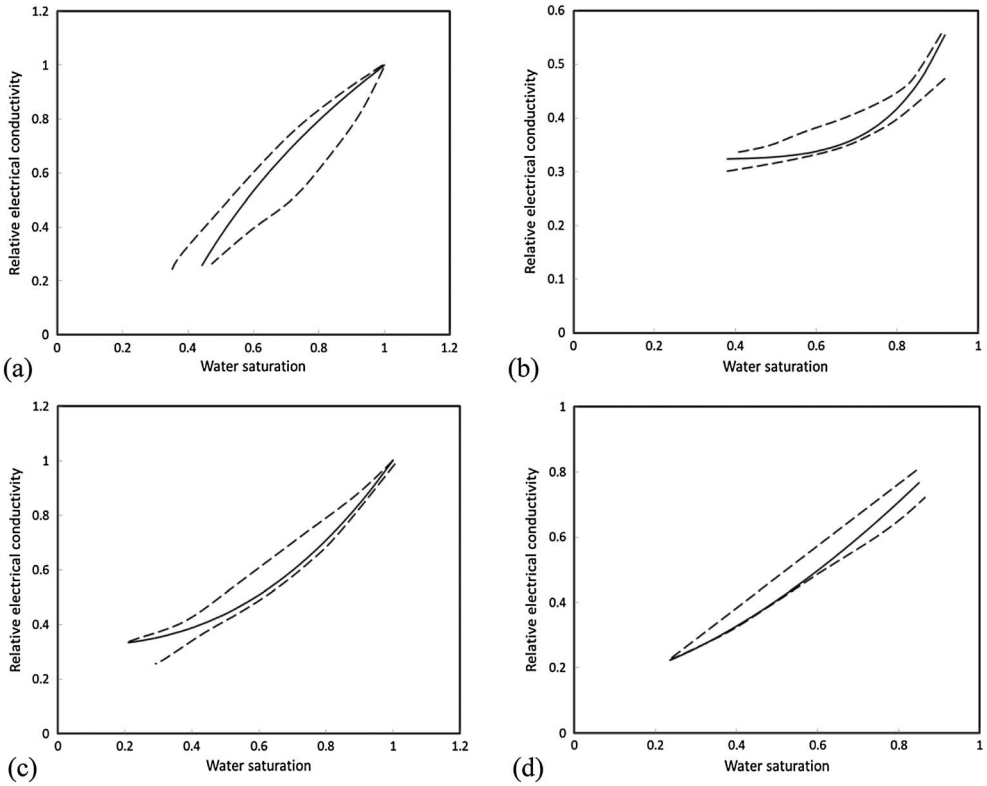

Figure 12. Summary results from the electrical conductivity optimization showing simulated data (solid lines) and variations (dashed lines). Relative electrical conductivity of the Stainton sample during (a) drainage and (b) imbibition; relative electrical conductivity of the St. Bees sample during (c) drainage and (d) imbibition.

here. We place a constraint that $p + r = 1$ because the relative streaming current charge density must equal 1 when the core sample is fully saturated with water. Values of p, q, and r obtained here are summarized in Table 5; the values are close regardless of sample for a given displacement, which suggests that the streaming current charge density is dictated by the pore-scale distribution of the two fluid phases. In the experiments reported here, this differs more significantly between drainage and imbibition than it does between the two sandstone samples for a given displacement, owing to the hysteresis in advancing and receding contact angles and differing pore-filling mechanisms [*Haines*, 1925; *Miller and Miller*, 1956].

Given the mismatch between measured and simulated electrical conductivity data at high water saturation discussed previously, we further tested higher-order polynomial functions and three-stage Archie-type functions for the electrical conductivity to determine whether changing the conductivity match significantly affected the streaming charge density and found that Q_r values remained within the range already determined. Thus, the small mismatch to the electrical conductivity at high water saturation has no significant influence on the Q_r model we proposed here.

4.2. Comparison of Our Model for Q_r Against Previous Studies

The model of the saturation dependence of the streaming current charge density we propose in equation (25) is compared with the models proposed by *Revil et al*. [2007] and *Jougnot et al*. [2012] in Figure 15. The model of *Jougnot et al*. [2012] was applied using our interpreted capillary pressure and relative permeability curves from the Stainton and St. Bees core samples and the WR and RP approaches. As discussed in section 1, the model of *Revil et al*. [2007] assumes that Q_r scales inversely with water saturation.

All three models predict that the relative streaming charge density increases monotonically with water saturation, but the $1/S_w$ model of *Revil et al*. [2007] predicts a lower streaming charge density at low water saturation when compared with our model and the model of *Jougnot et al*. [2012]; it also fails to capture

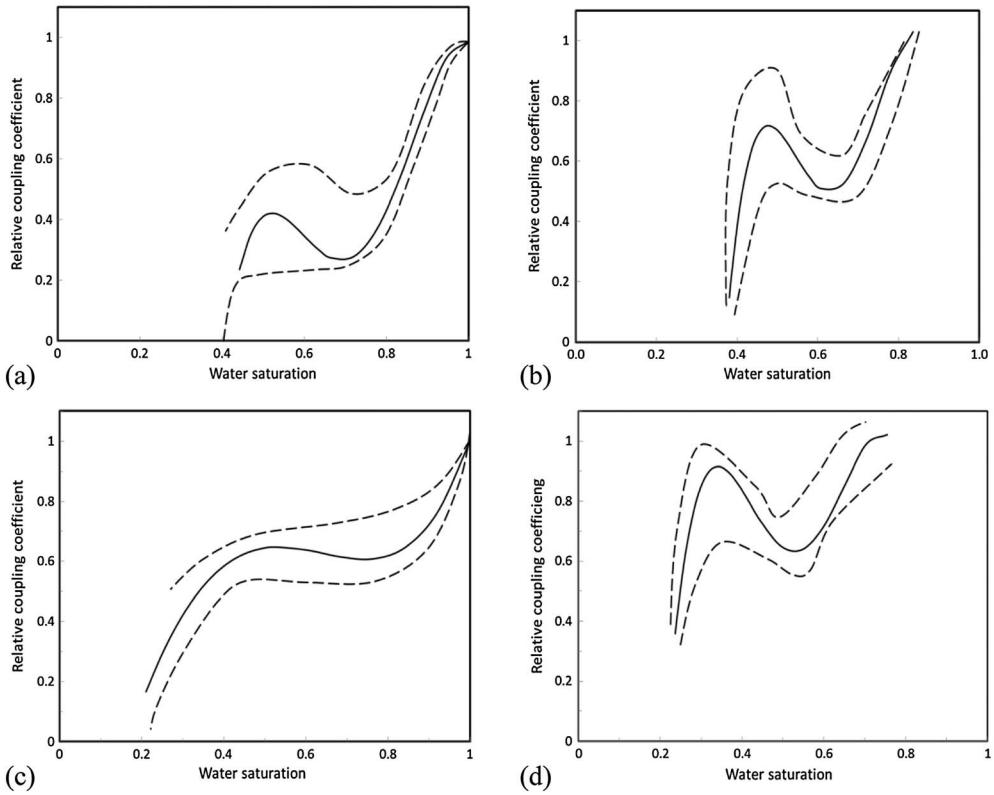

Figure 13. Summary results from the electrokinetic optimization showing simulated coupling coefficient and variations. Dash lines represent the ranges of the simulated coupling coefficient; solid lines are selected examples within the range; Relative coupling coefficient for the Stainton sample during (a) drainage and (b) imbibition; relative coupling coefficient for the St. Bees sample during (c) drainage and (d) imbibition.

Table 4. Ranges of Optimized Parameters From Hydraulic Conductivity, Electrical Conductivity, and Electrokinetic Optimization Steps

Hydraulic Optimization	Sample	α	β	A	λ	S_{wir}/S_{nwr}
Drainage	Stainton	3.332–4.003	2.005–3.716	0.010–0.199	6.000–10.472	0.374–0.442
	St. Bees	3.166–3.957	2.357–4.263	0.010–0.195	6.000–11.999	0.220–0.306
Imbibition	Stainton	2.008–3.250	2.002–3.651	8.718E−10–0.046	8.644–138.80	0.015–0.095
	St. Bees	2.000–2.755	2.392–4.946	3.269E−5–0.099	89.997–194.177	0.008–0.168
Electrical conductivity optimization		a_1 (S/m)		n	a_2 (S/m)	
Drainage	Stainton	0.015		1.267–1.771	-	
		0.009–0.011		2.843–3.541	0.004–0.006	
	St. Bees	0.018		0.874–0.938	-	
		0.012–0.014		1.518–1.677	0.004–0.005	
Imbibition	Stainton	0.006–0.007		0.401–0.598	-	
		0.006–0.008		6.123–7.946	0.004–0.005	
	St. Bees	0.013–0.016		0.527–0.899	-	
		0.010–0.015		1.219–2.412	0.003–0.005	
Electrokinetic optimization		b_1	b_2	b_3	b_4	b_5
Drainage	Stainton	−35.028 to 5.197	−0.015 to 41.856	−19.719 to 2.176	−0.312 to 7.200	0.132 to 0.457
	St. Bees	−17.037 to 6.609	−1.144 to 36.909	−24.446 to −3.692	−1.789 to 4.734	0.095 to 0.448
Imbibition	Stainton	−38.668 to −1.567	2.039 to 80.535	−53.759 to −1.470	−0.959 to 12.064	0.147 to 0.302
	St. Bees	−38.301 to 3.028	−11.260 to 72.741	−44.852 to 11.841	−3.125 to 9.961	0.210 to 0.465

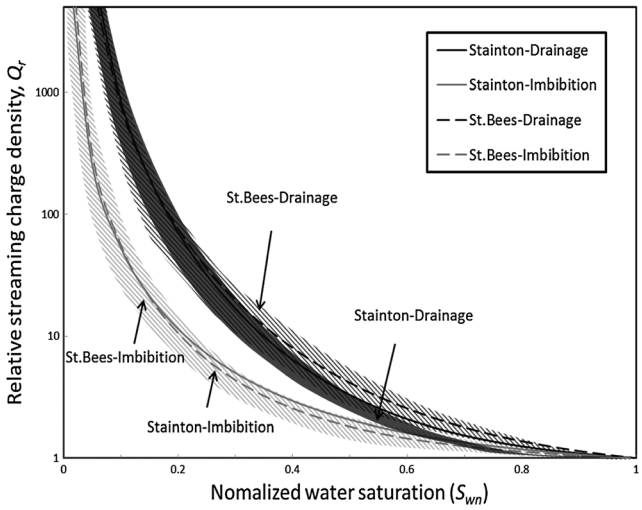

Figure 14. Relative streaming charge density as a function of normalized water saturation for Stainton (solid shaded area) and St. Bees (textured shaded area) during drainage (black) and imbibition (gray); the curves are given by our power law model for the relative streaming charge density (equation (25))) to fit the mean value of the optimized variations in each core and displacement (R^2 = 0.99999 in all cases). Fitting parameters p, q, and r are summarized in Table 5.

the hysteretic behavior between drainage and imbibition we observed here. However, in samples such as sandpacks with a narrow pore size distribution (such as a sand-pack), the $1/S_w$ model for Q_r may yield good predictions at high water saturation [*Linde et al*., 2007]. The model of *Jougnot et al*. [2012] predicts a similar exponential behavior of streaming charge density with normalized water saturation as obtained here. Comparing the two approaches in Figure 15, Q_r predicted using both the WR and RP approaches of *Jougnot et al*. [2012] demonstrates less hysteretic behavior and lower values of Q_r at intermediate and high water saturation than our interpreted data. We did not expect an exact fit, since the model of *Jougnot et al*. [2012] is based on a bundle of capillary tubes model, which is too simple to describe the pore structure of real rock.

4.3. Application of the Relative Streaming Current Charge Density Model to Predict the Relative Streaming Potential Coupling Coefficient

We now demonstrate the broad range of behaviors of the relative streaming potential coupling coefficient predicted using our model of the relative streaming current charge density (empirical values of sandstone average in Table 5 for equation (25)) in conjunction with a simple Corey model of relative permeability (equations (14) and (15)) and a simple Archie model for electrical conductivity (equation (20) with a_2 = 0). Recall that C_r is given by equation (12). We assume here that relative permeability, electrical conductivity, and streaming charge density are independent. This may not be the case, and attempts to relate electrical conductivity and permeability have been made [e.g., *Johnson et al*., 1987; *Revil and Cathles*, 1999; *Doussan and Ruy*, 2009]. However, any interdependencies for natural porous media are not well known [e.g., *Dullien*, 1992]. It is common to assume that relative permeability and electrical conductivity are independent, and they are often measured in separate experiments and on separate samples. Models for relative permeability and electrical conductivity also assume that they are independent.

Figure 16 shows the predicted C_r (S_w); the dashed lines denote the range of curves obtained using values of α and β (the Corey parameters) and n (the Archie parameter) varied in a simple Monte Carlo analysis over the range typically observed in water-wet rock (including the values determined for the two sandstones

Table 5. Values of Fitting Parameters (p, q, and r) of Relative Streaming Charge Density Functions With Water Saturation for Stainton and St. Bees During Drainage and Imbibition

Sample	Displacement process	p	q	r
Stainton	Drainage	0.201	−3.633	0.799
	Imbibition	0.275	−2.276	0.725
St. Bees	Drainage	0.340	−3.352	0.660
	Imbibition	0.174	−2.501	0.826
Sandstones (average)	Drainage	0.270	−3.493	0.729
	Imbibition	0.225	−2.388	0.775

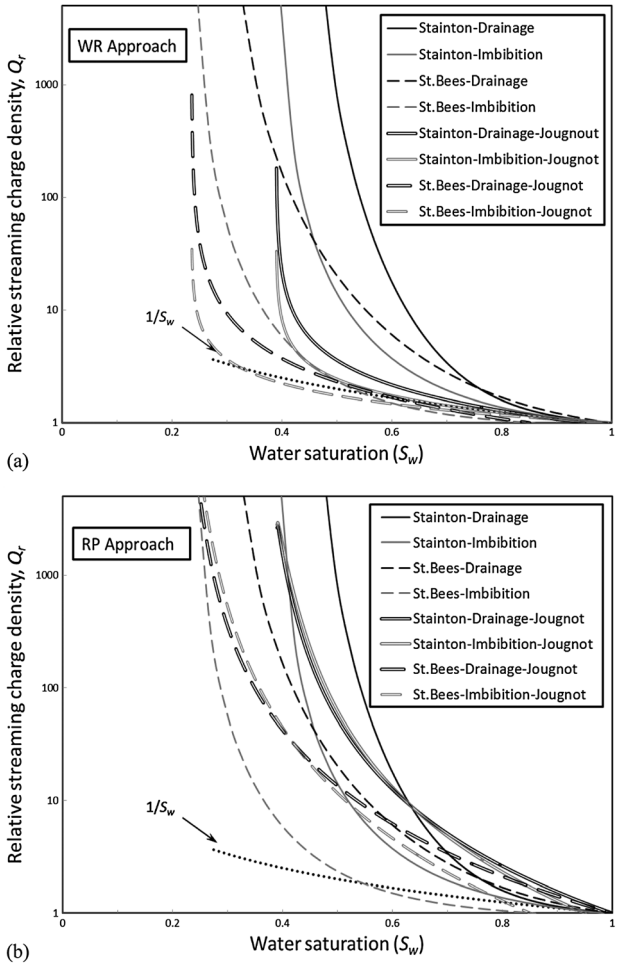

Figure 15. Predicted variation of streaming charge density with water saturation compared against other published models: solid and long dash lines are predicted using equation (25) and the values of *p*, *q*, and *r* reported in Table 5. The dotted line represents the model of *Revil et al*. [2007]. Models of *Jougnot et al*. [2012] for Stainton and St. Bees are also presented using using (a) WR and (b) RP approaches.

investigated here) and with arbitrarily chosen values of $S_{wir} = S_{nwr} = 0.2$ (note that $S_{nwr} = 0$ for drainage) (Figures 16a and 16b). We observe that depending on the parameters used, the Q_r model presented here yields both monotonic and nonmonotonic variations of C_r with S_w as observed experimentally (Figure 1). In contrast, the $1/S_w$ model predicts only monotonic variations in C_r. Complex behaviors as predicted in Figure 16 are also consistent with model predictions [*Jackson*, 2010; *Jougnot et al*., 2012] and seismoelectric laboratory measurements [*Bordes et al*., 2015]. Values of C_r can exceed 1 at partial saturation, although we cannot reproduce the large enhancements in C_r at partial saturation observed by *Allègre et al*. [2010].

We suggest that the broad range of behavior predicted here for reasonable models of k_r, σ_r, and Q_r may explain the contrasting and inconsistent experimental data reported to date (Figure 1). Small variations in the pore-scale distribution of the fluid phase cause variations in k_r, σ_r, and Q_r that yield complex and often nonmonotonic behavior of C_r. Indeed, our results suggest that the relative streaming current

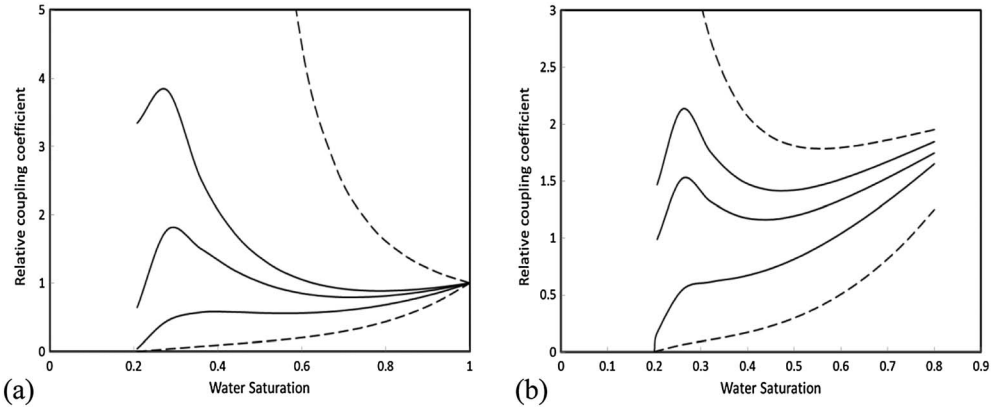

Figure 16. Predicted behavior of the relative streaming potential coupling coefficient using our model of the relative streaming charge (equation (25)) in conjunction with a simple Corey model of relative permeability (α and β over range 2–5) and a simple Archie model for electrical conductivity (*n* over range 1.5–3.5). Dash lines represent the ranges of the predicted coupling coefficient; solid lines are selected examples (a) during drainage and (b) during imbibition.

charge density may be similar for a given displacement (drainage or imbibition) and wetting state across different samples; variability in the relative streaming potential coupling coefficient arises primarily in response to variations in relative permeability and electrical conductivity.

4.4. Implications for Subsurface Flow Monitoring Using the SP and SE Methods

We propose here a simple empirical model for the saturation dependence of the relative streaming current charge density based on data interpreted from experiments on water-wet sandstones. These are the first data to be obtained using a method that makes no assumptions about the pore space geometry. The available data suggest that variability in Q_r across water-wet sandstones samples is small but that it is important to account for hysteresis between drainage and imbibition. However, further data are required to confirm this. Assuming a simple inverse water saturation function for Q_r does not account for hysteresis, yet such an approach has been applied in SP and SE studies of water-oil displacements which are dominated by forced or spontaneous imbibition rather than drainage (e.g., *Woodruff et al*. [2010] and *Revil et al*. [2014]; see *Saunders et al*. [2012] for a discussion of oil reservoir conditions relevant to SP).

The effect of wettability will be particularly important when predicting or modeling Q_r (S_w) (and hence C_r): *Jackson* [2010] used a capillary tubes model to show that wetting state will significantly impact on Q_r (S_w) if there is a difference in charge separation at the oil-water and mineral-water interfaces, while *Jackson and Vinogradov* [2012] measured streaming potential in water- and oil-wet carbonate samples at the residual oil saturation and found that the streaming current charge density in the oil-wet sample was 0 within experimental error. The saturation dependence of the streaming potential is therefore best determined by fitting a model (such as equation (25)) for the relative streaming current charge density to experimental data that specifically replicate the conditions of interest, particularly drainage versus imbibition and the wetting state. The saturation dependence of the streaming potential coupling coefficient is controlled by the saturation dependence of the relative permeability, electrical conductivity, and streaming current charge density, all of which depend on the conditions of interest and how these control the pore-scale distribution of the fluid phases.

5. Conclusions

We present (i) a method to interpret measurements of streaming potential in multiphase flow during unsteady state displacements of one fluid by another and (ii) application of the method to determine the saturation dependence of the streaming potential coupling coefficient (C) and streaming current charge density (Q_s) using experimental data obtained during drainage and imbibition in two different sandstone core samples.

We find that C exhibits hysteresis between drainage and imbibition, can exhibit significant nonmonotonic variations with saturation, is nonzero at the irreducible water saturation, and can exceed the value observed at $S_w = 1$. Moreover, Q_s also exhibits hysteresis, increasing with decreasing S_w but not as $1/S_w$ as is often assumed. The variation in Q_s with S_w is very similar for a given displacement for the two sandstone samples investigated, and we propose a simple empirical model for water-wet sandstones. The results presented here can be used to help interpret SP and SE measurements obtained in partially saturated subsurface settings.

We find that the streaming current charge density increases with water saturation (S_w) during both drainage and imbibition, but the relative streaming current charge density ($Q_r = Q(S_w)/Q(S_w = 1)$) is not given by $1/S_w$ as is often assumed. Rather, the variation of relative streaming charge density Q_r with S_w depends on the pore level distribution of water, which is controlled by rock texture and wettability and is different for the two sandstone samples investigated here. Our results show that C (S_w) exhibits complex, nonmonotonic behavior, depending upon the (monotonic) saturation dependence of relative permeability, relative electrical conductivity, and relative streaming current charge density.

Acknowledgments
TOTAL is thanked for partially funding Jackson under the TOTAL Chairs programme at Imperial College London and for funding Vinogradov. Shell is thanked for funding Leinov. The Department of Earth Science and Engineering at Imperial College London is thanked for supporting Zhang with a Janet Watson Scholarship. Damien Jougnot, Frederic Perrier, and an anonymous reviewer are thanked for their careful and thorough reviews. The data for this paper are available in supporting information or by contacting the corresponding author m.d.jackson@imperial.ac.uk.

References

Allègre, V., L. Jouniaux, F. Lehmann, and P. Sailhac (2010), Streaming potential dependence on water-content in Fontainebleau sand, *Geophys. J. Int.*, *182*(3), 1248–1266, doi:10.1111/j.1365-246X.2010.04716.x.

Allègre, V., L. Jouniaux, F. Lehmann, and P. Sailhac (2011), Reply to comment by A. Revil and N. Linde on 'Streaming potential dependence on water-content in Fontainebleau sand', *Geophys. J. Int.*, *186*(1), 115–117, doi:10.1111/j.1365-246X.2011.05038.x.

Allègre, V., A. Maineult, F. Lehmann, F. Lopes, and M. Zamora (2014), Self-potential response to drainage–imbibition cycles, *Geophys. J. Int.*, *197*(3), 1410–1424, doi:10.1093/gji/ggu055.
Antraygues, P., and M. Aubert (1993), Self potential generated by two-phase flow in a porous medium: Experimental study and volcanological applications, *J. Geophys. Res.*, *98*(B12), 22,273–22,281, doi:10.1029/93JB02395.
Blunt, M. J., M. D. Jackson, M. Piri, and P. H. Valvatne (2002), Detailed physics, predictive capabilities and macroscopic consequences for pore-network models of multiphase flow, *Adv. Water Resour.*, *25*(8), 1069–1089.
Bordes, C., P. Sénéchal, J. Barrière, D. Brito, E. Normandin, and D. Jougnot (2015), Impact of water saturation on seismoelectric transfer functions: A laboratory study of coseismic phenomenon, *Geophys. J. Int.*, *200*(3), 1317–1335.
Brooks, R. H., and A. T. Corey (1964), Hydraulic properties of porous media and their relation to drainage design, *Trans. ASAE*, *7*(1), 26–0028.
Clavier, C., G. Coates, and J. Dumanoir (1984), Theoretical and experimental bases for the dual-water model for interpretation of shaly sands, *SPE J.*, *24*, 153–168, doi:10.2118/6859-PA.
Corwin, R., and D. Hoover (1979), The self-potential method in geothermal exploration, *Geophysics*, *44*(2), 226–245, doi:10.1190/1.1440964.
Darnet, M., and G. Marquis (2004), Modelling streaming potential (SP) signals induced by water movement in the vadose zone, *J. Hydrol.*, *285*(1), 114–124, doi:10.1016/j.jhydrol.2003.08.010.
Darnet, M., A. Maineult, and G. Marquis (2004), On the origins of self-potential (SP) anomalies induced by water injections into geothermal reservoirs, *Geophys. Res. Lett.*, *31*, L19609, doi:10.1029/2004GL020922.
Doussan, C., and S. Ruy (2009), Prediction of unsaturated soil hydraulic conductivity with electrical conductivity, *Water Resour. Res.*, *45*, W10408, doi:10.1029/2008WR007309.
Doussan, C., L. Jouniaux, and J.-L. Thony (2002), Variations of self-potential and unsaturated water flow with time in sandy loam and clay loam soils, *J. Hydrol.*, *267*(3–4), 173–185, doi:10.1016/S0022-1694(02)00148-8.
Dullien, F. A. L. (1992), *Porous Media: Fluid Transport and Pore Structure*, pp. 333–478, Academic Press, Univ. of Calif.
Fenwick, D. H., and M. J. Blunt (1998), Three-dimensional modeling of three phase imbibition and drainage, *Adv. Water Resour.*, *21*(2), 121–143, doi:10.1016/S0309-1708(96)00037-1.
Glover, P. W. J., M. J. Hole, and J. Pous (2000), A modified Archie's law for two conducting phases, *Earth Planet. Sci. Lett.*, *180*(3–4), 369–383, doi:10.1016/S0012-821X(00)00168-0.
Guichet, X., L. Jouniaux, and J.-P. Pozzi (2003), Streaming potential of a sand column in partial saturation conditions, *J. Geophys. Res.*, *108*(B3), 2141, doi:10.1029/2001JB001517.
Gulamali, M., E. Leinov, and M. Jackson (2011), Self-potential anomalies induced by water injection into hydrocarbon reservoirs, *Geophysics*, *76*(4), F283–F292, doi:10.1190/1.3596010.
Haines, W. B. (1925), Studies in the physical properties of soils: III. Observations on the electrical conductivity of soils, *J. Agric. Sci.*, *15*(04), 536–543, doi:10.1017/S0021859600082472.
Hearst, J. R., and P. H. Nelson (1985), *Well Logging for Physical Properties*, pp. 447–473, McGraw-Hill, New York.
Ishido, T., and H. Mizutani (1981), Experimental and theoretical basis of electrokinetic phenomena in rock-water systems and its applications to geophysics, *J. Geophys. Res.*, *86*(B3), 1763–1775, doi:10.1029/JB086iB03p01763.
Jackson, M. D. (2008), Characterization of multiphase electrokinetic coupling using a bundle of capillary tubes model, *J. Geophys. Res.*, *113*, B04201, doi:10.1029/2007JB005490.
Jackson, M. D. (2010), Multiphase electrokinetic coupling: Insights into the impact of fluid and charge distribution at the pore scale from a bundle of capillary tubes model, *J. Geophys. Res.*, *115*, B07206, doi:10.1029/2009JB007092.
Jackson, M. D., and J. Vinogradov (2012), Impact of wettability on laboratory measurements of streaming potential in carbonates, *Colloids Surf., A*, *393*, 86–95.
Jackson, M. D., J. H. Saunders, and E. Addiego-Guevara (2005), Development and application of new downhole technology to detect water encroachment toward intelligent wells, SPE Annual Technical Conference and Exhibition, Soc. of Pet. Eng.
Joekar-Niasar, V., and S. M. Hassanizadeh (2011), Effect of fluids properties on non-equilibrium capillarity effects: Dynamic pore-network modeling, *Int. J. Multiphase Flow*, *37*(2), 198–214.
Johnson, D. L., T. J. Plona, and H. Kojima (1987), Probing porous media with 1st sound, 2nd sound, 4th sound, and 3rd sound, *AIP Conf. Proc.*, *154*(1), 243–277, doi:10.1063/1.36398.
Jougnot, D., N. Linde, A. Revil, and C. Doussan (2012), Derivation of soil-specific streaming potential electrical parameters from hydrodynamic characteristics of partially saturated soils, *Vadoze Zone J.*, *11*(1), 1–15, doi:10.2136/vzj2011.0086.
Jougnot, D., N. Linde, E. B. Haarder, and M. C. Looms (2015), Monitoring of saline tracer movement with vertically distributed self-potential measurements at the HOBE agricultural test site, Voulund, Denmark, *J. Hydrol.*, *521*, 314–327, doi:10.1016/j.jhydrol.2014.11.041.
Jouniaux, L., and J.-P. Pozzi (1995), Streaming potential and permeability of saturated sandstones under triaxial stress: Consequences for electrotelluric anomalies prior to earthquakes, *J. Geophys. Res.*, *100*(B6), 10,197–10,209, doi:10.1029/95JB00069.
Knackstedt, M. A., C. H. Arns, A. P. Sheppard, T. J. Senden, R. M. Sok, Y. Cinar, W. V. Pinczewski, M. Ioannidis, and G. S. Padhy (2007), Archie's exponents in complex lithologies derived from 3D digital core analysis, in *SPWLA 48th Annual Logging Symposium*, edited, Soc. of Petrophysicists and Well-Log Anal., Austin, Tex.
Knight, R. (1991), Hysteresis in the electrical resistivity of partially saturated sandstones, *Geophysics*, *56*(12), 2139–2147.
Kulessa, B., D. Chandler, A. Revil, and R. Essery (2012), Theory and numerical modeling of electrical self-potential signatures of unsaturated flow in melting snow, *Water Resour. Res.*, *48*, W09511, doi:10.1029/2012WR012048.
Leverett, M. C. (1942), Capillary behavior in porous solids, *Trans. AIME*, *142*(1), 152–169, doi:10.2118/941152-G.
Linde, N. (2009), Comment on "Characterization of multiphase electrokinetic coupling using a bundle of capillary tubes model" by Mathew D. Jackson, *J. Geophys. Res.*, *114*, B06209, doi:10.1029/2008JB005845.
Linde, N., D. Jougnot, A. Revil, S. K. Matthäi, T. Arora, D. Renard, and C. Doussan (2007), Streaming current generation in two-phase flow conditions, *Geophys. Res. Lett.*, *34*, L03306, doi:10.1029/2006GL028878.
Longeron, D. G., M. J. Argaud, and J. P. Feraud (1989), Effect of overburden pressure and the nature and microscopic distribution of fluids on electrical properties of rock samples, *SPE Form. Eval.*, *4*(2), 194–202, doi:10.2118/15383-PA.
MATLAB (2012), Version 8.0.0.783 (R2012b), The MathWorks Inc., Natick, Mass.
Miller, E. E., and R. D. Miller (1956), Physical theory for capillary flow phenomena, *J. Appl. Phys.*, *27*(4), 324–332, doi:10.1063/1.1722370.
Moore, J. R., S. D. Glaser, H. F. Morrison, and G. M. Hoversten (2004), The streaming potential of liquid carbon dioxide in Berea sandstone, *Geophys. Res. Lett.*, *31*, L17610, doi:10.1029/2004GL020774.
Nocedal, J., and S. Wright (2006), *Numerical Optimization*, Springer.
Perrier, F., and P. Morat (2000), Characterization of electrical daily variations induced by capillary flow in the non-saturated zone, *Pure Appl. Geophys.*, *157*(5), 785–810, doi:10.1007/PL00001118.

Revil, A. (1999), Ionic diffusivity, electrical conductivity, membrane and thermoelectric potentials in colloids and granular porous media: A unified model, *J. Colloid Interface Sci.*, *212*(2), 503–522.
Revil, A., and L. M. Cathles (1999), Permeability of shaly sands, *Water Resour. Res.*, *35*(3), 651–662, doi:10.1029/98WR02700.
Revil, A., and A. Cerepi (2004), Streaming potentials in two-phase flow conditions, *Geophys. Res. Lett.*, *31*, L11605, doi:10.1029/2004GL020140.
Revil, A., and P. W. J. Glover (1998), Nature of surface electrical conductivity in natural sands, sandstones, and clays, *Geophys. Res. Lett.*, *25*(5), 691–694, doi:10.1029/98GL00296.
Revil, A., N. Linde, A. Cerepi, D. Jougnot, S. Matthäi, and S. Finsterle (2007), Electrokinetic coupling in unsaturated porous media, *J. Colloid Interface Sci.*, *313*(1), 315–327, doi:10.1016/j.jcis.2007.03.037.
Revil, A., G. Barnier, M. Karaoulis, P. Sava, A. Jardani, and B. Kulessa (2014), Seismoelectric coupling in unsaturated porous media: Theory, petrophysics, and saturation front localization using an electroacoustic approach, *Geophys. J. Int.*, *196*(2), 867–884, doi:10.1093/gji/ggt440.
Roberts, J. J., and W. Lin (1997), Electrical properties of partially saturated Topopah Spring Tuff: Water distribution as a function of saturation, *Water Resour. Res.*, *33*(4), 577–587, doi:10.1029/96WR03905.
Saunders, J. H., M. D. Jackson, and C. C. Pain (2006), A new numerical model of electrokinetic potential response during hydrocarbon recovery, *Geophys. Res. Lett.*, *33*, L15316, doi:10.1029/2006GL026835.
Saunders, J. H., M. D. Jackson, and C. C. Pain (2008), Fluid flow monitoring in oil fields using downhole measurements of electrokinetic potential, *Geophysics*, *73*(5), E165–E180, doi:10.1190/1.2959139.
Saunders, J. H., M. D. Jackson, M. Y. Gulamali, J. Vinogradov, and C. C. Pain (2012), Streaming potentials at hydrocarbon reservoir conditions, *Geophysics*, *77*(1), E77–E90, doi:10.1190/geo2011-0068.1.
Schittkowski, K. (1985), User's guide for the nonlinear programming code NLPQL, in *Handbook to Optimization Program Package NLPQL*, vol. 3, pp. 3–2 Univ. of Stuttgart-Inst. for Inf., Germany.
Schlumberger (2013), ECLIPSE techinical description 2013.1: Schlumberger, Telford, W. M., Geldart, L.P., Sheriff, R.E., 1990, Applied geophysics, 2nd ed., Cambridge Univ. Press.
Sigmund, P. M., and F. G. McCaffery (1979), An improved unsteady-state procedure for determining the relative-permeability characteristics of heterogeneous porous media (includes associated papers 8028 and 8777), *Soc. Pet. Eng. J.*, *19*(1), 15–28, doi:10.2118/6720-PA.
Sill, W. (1983), Self-potential modeling from primary flows, *Geophysics*, *48*(1), 76–86, doi:10.1190/1.1441409.
Suman, R. J., and R. Knight (1997), Effects of pore structure and wettability on the electrical resistivity of partially saturated rocks—A network study, *Geophysics*, *62*(4), 1151–1162, doi:10.1190/1.1444216.
Talebian, M., R. Al-Khoury, and L. J. Sluys (2013), Coupled electrokinetic–hydromechanic model for \text{ CO}_{2} sequestration in porous media, *Transp. Porous Media*, *98*(2), 287–321, doi:10.1007/s11242-013-0145-y.
Titov, K., Y. Ilyin, P. Konosavski, and A. Levitski (2002), Electrokinetic spontaneous polarization in porous media: Petrophysics and numerical modelling, *J. Hydrol.*, *267*(3–4), 207–216, doi:10.1016/S0022-1694(02)00151-8.
Vinogradov, J., and M. D. Jackson (2011), Multiphase streaming potential in sandstones saturated with gas/brine and oil/brine during drainage and imbibition, *Geophys. Res. Lett.*, *38*, L01301, doi:10.1029/2010GL045726.
Warden, S., S. Garambois, L. Jouniaux, D. Brito, P. Sailhac, and C. Bordes (2013), Seismoelectric wave propagation numerical modelling in partially saturated materials, *Geophys. J. Int.*, doi:10.1093/gji/ggt198.
Woodruff, W. F., A. Revil, A. Jardani, D. Nummedal, and S. Cumella (2010), Stochastic Bayesian inversion of borehole self-potential measurements, *Geophys. J. Int.*, *183*(2), 748–764, doi:10.1111/j.1365-246X.2010.04770.x.
Wurmstich, B., and F. Morgan (1994), Modeling of streaming potential responses caused by oil well pumping, *Geophysics*, *59*(1), 46–56, doi:10.1190/1.1443533.